Direct Comparison of PdAu Alloy Thin Films and Nanoparticles upon Hydrogen Exposure

ACS APPLIED MATERIALS & INTERFACES

Research Article

Cite This: ACS Appl. Mater. Interfaces 2019, 11, 15489−15497

www.acsami.org

Direct Comparison of PdAu Alloy Thin Films and Nanoparticles upon Hydrogen Exposure

Lars Johannes Bannenberg,*[,†] Ferry Anggoro Ardy Nugroho,[‡] Herman Schreuders,[†] Ben Norder,[†] Thu Trang Trinh,[§] Nina-Juliane Steinke,[∥] Ad A. van Well,[†] Christoph Langhammer,[‡] and Bernard Dam*[,†]

[†]Faculty of Applied Sciences, Delft University of Technology, Mekelweg 15, 2629 JB Delft, The Netherlands

[‡]Department of Physics, Chalmers University of Technology, 412 96 Göteborg, Sweden

[§]Helmholtz-Zentrum Dresden-Rossendorf, DE 01328 Dresden, Germany

[∥]ISIS Neutron Source, Rutherford Appleton Laboratory, STFC, OX11 0QX Didcot, U.K.

Supporting Information

ABSTRACT: Nanostructured metal hydrides are able to efficiently detect hydrogen in optical sensors. In the literature, two nanostructured systems based on metal hydrides have been proposed for this purpose each with its own detection principle: continuous sub-100 nm thin films read out via optical reflectance/transmittance changes and nanoparticle arrays for which the detection relies on localized surface plasmon resonance. Despite their apparent similarities, their optical and structural response to hydrogen has never been directly compared. In response, for the case of $Pd_{1-y}Au_y$ (y = 0.15−0.30) alloys, we directly compare these two systems and establish that they are distinctively different. We show that the dissimilar optical response is not caused by the different optical readout principles but results from a fundamentally different structural response to hydrogen due to the different nanostructurings. The measurements empirically suggest that these differences cannot be fully accounted by surface effects but that the nature of the film−substrate interaction plays an important role and affects both the hydrogen solubility and the metal-to-metal hydride transition. In a broader perspective, our results establish that the specifics of nanoconfinement dictate the structural properties of metal hydrides, which in turn control the properties of nanostructured devices including the sensing characteristics of optical hydrogen sensors and hydride-based active plasmonic systems.

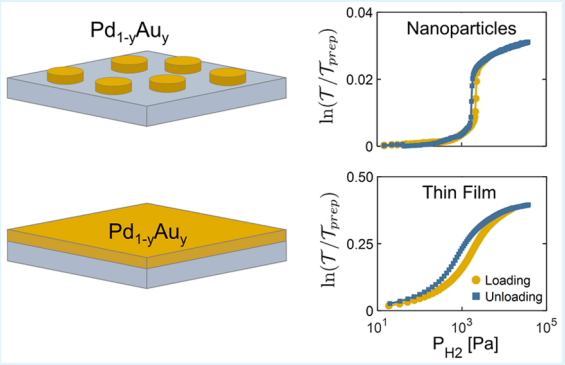

KEYWORDS: *nanostructuring, optical hydrogen sensing, metal hydride, plasmonics, thin films, nanoparticles, PdAu, X-ray diffraction*

INTRODUCTION

The detection of hydrogen in a fast, reliable, and accurate manner is key for its safe handling in industrial processes and for its acceptance and implementation as an energy vector. In this context, optical hydrogen sensors have an inherent safety benefit because they do not require electrical contacts which may introduce sparks near the sensing area. In addition, they can be made small, relatively cheap and offer the possibility to spatially separate the readout from the sensing area.[1−8]

To this end, two different nanoarchitectures have been proposed to optically track hydrogen: continuous thin films[2,3,5,6,9] and arrays of nanosized particles.[8,10] Both of these systems take advantage of a metal hydride-based sensing material, which hydrogenates upon an increase in partial hydrogen pressure, resulting in the change of its optical properties.[11] However, the underlying physics of the generated optical contrast and signal readout of the two systems differs substantially. Whereas the readout of thin film sensors typically relies on changes in the optical reflectance or transmittance, the readout of nanoparticles relies on the excitation of localized surface plasmon resonances (LSPR) and the tracking of the corresponding "peak" in the optical spectrum, which broadens and shifts to longer wavelengths upon hydrogen sorption.[10]

In the field of hydrogen sensors, PdAu alloys have, in particular, been considered as an effective sensing material for both thin films[12−14] and nanoparticles.[15−20] The alloying of the reference metal hydride palladium with gold significantly reduces or even completely eliminates the undesirable hysteresis from the first order metal-to-metal hydride transition, while it maintains the ability to dissociate hydrogen at room temperatures.[21,22] A naive comparison of different studies of PdAu indicates that the performance in terms of hysteresis, sensing range, and sensitivity of thin film and nanoparticle based sensors is, quite surprisingly, substantially

Received: December 31, 2018
Accepted: April 8, 2019
Published: April 8, 2019

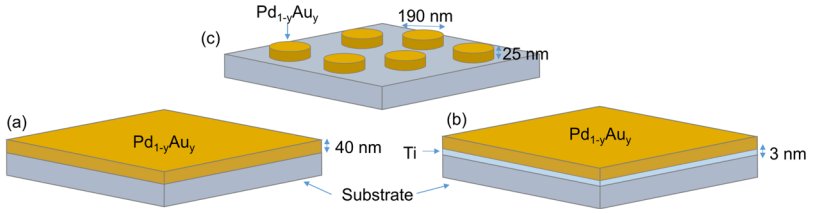

Figure 1. Schematic illustration of the samples studied: (a) 40 nm $Pd_{1-y}Au_y$ continuous thin film deposited on quartz substrates, (b) 40 nm $Pd_{1-y}Au_y$ continuous thin film with an additional 3 nm Ti adhesion layer, and (c) disk-shaped $Pd_{1-y}Au_y$ nanoparticles with a diameter of 190 nm and a thickness of 25 nm.

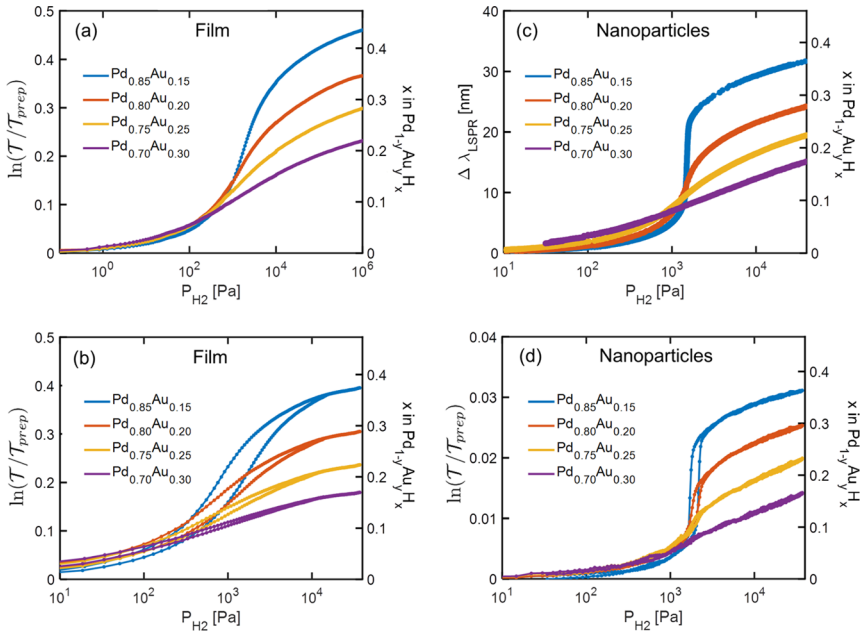

Figure 2. Partial hydrogen pressure and composition dependence of the optical readout of $Pd_{1-y}Au_y$ (y = 0.15−0.30) (a,b) thin films and (c,d) nanoparticles at T = 28 °C. (a) Pressure dependence of the changes in optical transmission of the $Pd_{1-y}Au_y$ thin films as measured relative to the optical transmission of the as-prepared sample ($\mathcal{T}_{prep}$) and by stepwise increasing the pressure. (b) Pressure dependence of the changes in optical transmission of the $Pd_{1-y}Au_y$ thin films in the intermediate pressure region where hysteresis occurs. The optical transmission was measured by stepwise increasing and decreasing the pressure between $P_{H_2} = 1 \times 10^{-1}$ and 4×10^5 Pa. (c) Pressure dependence of the shift of the LSPR with respect to the as-prepared sample $\Delta\lambda_{LSPR}$ of the $Pd_{1-y}Au_y$ nanoparticles as measured by stepwise increasing the pressure. (d) Pressure dependence of the changes in optical transmission of the $Pd_{1-y}Au_y$ nanoparticles relative to the optical transmission of the as-prepared sample ($\mathcal{T}_{prep}$) measured by stepwise increasing and decreasing the pressure between $P_{H_2} = 1 \times 10^{-1}$ and 4×10^5 Pa. The right vertical axis of all subfigures indicates x in $Pd_{1-y}Au_yH_x$ based on the scaling between the optical response and the hydrogen content of the alloy (see Figure 3).

different.[13,17,19] However, no explicit comparison has been made and it therefore remains unclear whether these deviations in performance have purely an experimental origin (e.g., different ways of preparing the alloy or different Au concentrations) are caused by different structural responses to hydrogen, or if they stem from the fundamentally different nature of the involved optical excitations and thus the interaction of light with the hydride in a thin film or in a nanoparticle.

To explicitly address this question, which is not only of fundamental importance but also of practical relevance for successfully applying metal hydrides in, for example, next generation hydrogen sensors, this paper makes an explicit comparison between the optical response of $Pd_{1-y}Au_y$ (y = 0.15−0.30) 40 nm thick thin films and 190 nm diameter disk-shaped nanoparticles, as illustrated in Figure 1, when exposed to hydrogen. As the key results, by means of neutron reflectometry (NR) and quartz-crystal microbalance (QCM) measurements, we find a linear relation between the optical signal and the amount of hydrogen absorbed for both systems, and our analysis shows that the hydrogen solubility in the metal phase is significantly enhanced for the thin films compared to nanoparticles and bulk $Pd_{1-y}Au_y$. Furthermore, in situ X-ray diffraction (XRD) reveals that the origin of hysteresis in nanoparticles with Au concentrations up to y = 0.15 is an incoherent first-order transition between the dilute α-$Pd_{1-y}Au_yH_x$ and high hydrogen concentration β-$Pd_{1-y}Au_yH_x$ phases. In contrast, in the corresponding thin film system, no signature of an incoherent phase transition is seen, however, substantial hysteresis is observed which persists up to y = 0.30 and spans a much wider pressure range. Because the diffractograms do not show two-phase behavior, we attribute the hysteresis purely to the plastic deformation due to substantial surface-clamping effects for thin films. These results highlight that the specifics of nanoconfinement dictate the structural properties of metal hydrides, which in turn controls the properties of nanostructured hydride-based devices, such as

DOI: 10.1021/acsami.8b22455
ACS Appl. Mater. Interfaces 2019, 11, 15489−15497

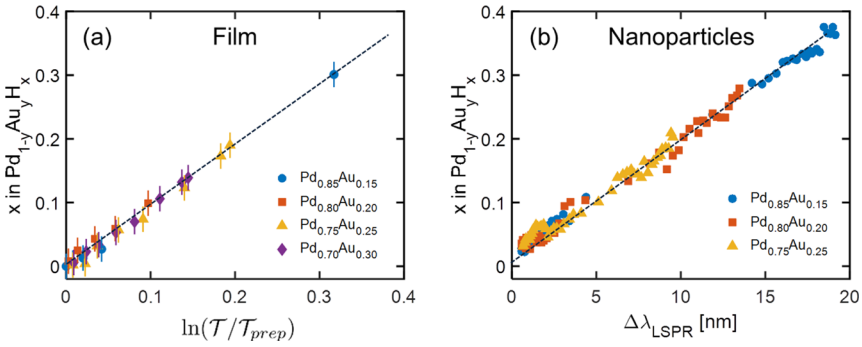

Figure 3. Relation between the optical readout and x in $Pd_{1-y}Au_yH_x$ for $Pd_{1-y}Au_yH_x$ (y = 0.15−0.30) thin films and nanoparticles. (a) x in $Pd_{1-y}Au_yH_x$ for $Pd_{1-y}Au_yH_x$ thin films as a function of the changes in optical transmission relative to the optical transmission of the as-prepared sample ($\mathcal{T}_{prep}$). (b) x in $Pd_{1-y}Au_yH_x$ for $Pd_{1-y}Au_yH_x$ nanoparticles as a function of the wavelength shift of the LSPR with respect to the as-prepared state $\Delta\lambda_{LSPR}$ after ref 19.

the sensing characteristics of optical hydrogen sensors and hydride-based active plasmonic sensors.

OPTICAL MEASUREMENTS

Figure 2 summarizes the partial hydrogen pressure and composition dependence of the optical readout of thin films and nanoparticles of $Pd_{1-y}Au_y$ (y = 0.15−0.30) at T = 28 °C. For thin films, we display in Figure 2a,b the change in the white light optical transmission of the film, $\mathcal{T}$, upon hydrogen exposure, relative to the transmission of the as-prepared sample $\mathcal{T}_{prep}$. We have considered both thin films without [Figure 1a] and with a 3 nm adhesion layer [Figure 1b], and as discussed in the Methods and Materials section, they feature highly similar results from the second hydrogenation onward. For the nanoparticles (grown without adhesion layer, Figure 1c), we display in Figure 2c the wavelength shift of the LSPR peak, $\Delta\lambda_{LSPR}$, with respect to the metallic state ($P_{H_2} < 5 \times 10^{-4}$ Pa).

The optical results are in good agreement with the literature,[13,17,19] and reproduce the key features, that is, for both thin films and nanoparticles, the optical contrast and hysteresis upon exposure to hydrogen decreases with increasing gold concentrations. In particular, all compositions of the thin films and nanoparticles show a pronounced and monotonous optical response to the partial hydrogen pressures over a wide range of $1 \le P_{H_2} \le 1 \times 10^6$ Pa. As the upper limit of the sensing ranges of both $Pd_{1-y}Au_y$ thin films and nanoparticles are limited by the maximum pressure accessible in our experimental setups, we conjecture that it may extend to (much) higher hydrogen pressures.

Interestingly, however, the optical measurements also clearly show dissimilarities between the two systems with respect to the: (1) sensitivity and (2) appearance of hysteresis. With respect to (1), the optical response to hydrogen is more gradual in thin films. On the other hand, the $Pd_{1-y}Au_y$ nanoparticles show, especially at low Au concentrations, a more steplike response of $\Delta\lambda_{LSPR}$ as a function of the hydrogen pressure, whereas the response of the two systems becomes more similar at higher Au concentrations.

With respect to (2), we observe hysteresis in the optical response of the $Pd_{1-y}Au_y$ thin films across a wide pressure range which diminishes with increasing Au concentration and with increasing temperature [Figure S1]. However, it persists even for $Pd_{0.70}Au_{0.30}$. In contrast, hysteresis in the optical readout of the nanoparticles is limited to $Pd_{1-y}Au_y$ with y = 0.15, 0.20, and 0.25 while it is completely absent at y = 0.30. Furthermore, it occurs only in a narrow pressure region centered around $P_{H_2} = 2 \times 10^3$ Pa, that is, around the plateau pressure of bulk palladium.[22] Consistent with previous research,[23] we note that the disappearance of hysteresis for alloys with higher Au content occurs at lower temperatures, indicating a lower critical temperature [Figure S2].

The next step in the analysis is to establish whether the differences between the optical response of $Pd_{1-y}Au_y$ (y = 0.15−0.30) thin films and nanoparticles to hydrogen originates from the different detection mechanisms that create the optical contrast, that is, light attenuation versus excitation of LSPR. We do so by measuring the optical transmission of the $Pd_{1-y}Au_y$ nanoparticles using the same setups and procedures as the ones used for the thin film measurements. Figure 2d shows that the partial hydrogen pressure dependence of $\ln(\mathcal{T}/\mathcal{T}_{prep})$ is qualitatively very similar to that of $\Delta\lambda_{LSPR}$. Hence, clearly the differences between the $Pd_{1-y}Au_y$ thin films and nanoparticles are not the result of the optical detection method but likely relate to different structural and thermodynamic properties, as we discuss below. In addition, these results illustrate that one may track the optical transmission of nanoparticles as alternative readout to $\Delta\lambda_{LSPR}$, while maintaining its desirable properties in terms of limited-to-no hysteresis and fast response times.[17]

STRUCTURAL MEASUREMENTS

Hydrogen Solubility. To evaluate whether the difference in response is related to dissimilar hydrogen solubility in the two systems, we examine the pressure dependence of the hydrogen content in $Pd_{1-y}Au_y$ thin films by NR (thin films) and compare it to the one in nanoparticles recently established using a QCM.[19] By comparing these data [Figures S3 and S4] with the optical measurements, we establish an important relation: in all cases, the optical response, either the change in the white light transmission or the wavelength shift of the LSPR peak, scales linearly and universally with the absolute amount of hydrogen content irrespective of the Au fractions in the alloy [Figure 3]. Such a linear scaling has been reported before for other pure metal hydrides,[9,19,24,25] but its appearance and especially the universality is not at all trivial. One might expect that this universal scaling holds in the case of a coexistence of two phases with varying fractions, but it is not directly clear why it holds in the present situation of an increasing hydrogen content in a solid solution of palladium−gold and hydrogen. In addition, a comparison of the magnitude

DOI: 10.1021/acsami.8b22455
ACS Appl. Mater. Interfaces 2019, 11, 15489−15497

of the changes in optical transmission of the thin films upon hydrogenation [Figure 2a] with the one of nanoparticles [Figure 2d] yields that, for a given hydrogen content, the change in optical transmission with respect to the unloaded state is for all compositions about 10 times larger for the thin films. This difference can be fully accounted for by the different coverage fraction of the substrate (≈15% instead of 100%) and thickness of the layer (25 nm instead of 40 nm) of the nanoparticles with respect to that of the thin film, confirming that the absolute amount of hydrogen absorbed by the metallic host dictates the change in optical transmission. The results empirically suggest that the effect of hydrogen on the optical properties is independent of (i) its concentration and (ii) the composition of the metallic host, that is, the gold concentration. The universal scaling between the optical response and hydrogen content has the convenient implication that one can infer the hydrogen content from the optical response for thin films/nanoparticles with the same thickness. Therefore, this allows us also to present the hydrogen content of the alloy on the right *y*-axes of Figure 2.

A second interesting aspect, the direct comparison of the hydrogen solubilities in $Pd_{1-y}Au_y$ thin films and nanoparticles with the data for bulk $Pd_{1-y}Au_y$ from ref 22, as displayed in Figure 4 for the case of $Pd_{0.85}Au_{0.15}$, reveals that thin films

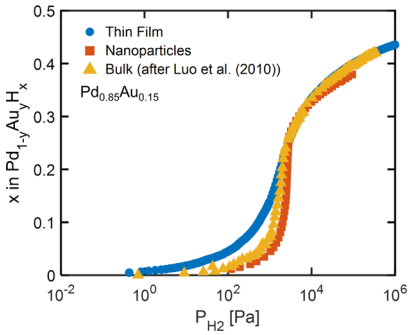

Figure 4. Comparison of the hydrogen solubility of a thin film (T = 28 °C), a nanoparticle thin film (T = 28 °C) and bulk material (T = 30 °C) of $Pd_{0.85}Au_{0.15}$. The measurements were performed by stepwise increasing the hydrogen pressure. The bulk data are adapted from ref 22.

exhibit a higher hydrogen solubility than both nanoparticles and bulk. This not only explains the observed larger optical contrast (and thus sensitivity in a sensor application) of the thin films in the low hydrogen pressure regime [Figure 2a] but also allows us to draw an important conclusion: although size dependencies of the hydrogen solubility in metal hydrides have been reported before (see, e.g., refs[26−28]), these results empirically suggest that the enhanced solubility of hydrogen at low hydrogen pressures for thin films is not solely the result of interface/surface effects because such effects should be comparable or even more pronounced for nanoparticles. Hence, as further elaborated below, we postulate that the enhanced solubility observed in thin films is related to the compression exerted by the clamping effect of the substrate, which is very sizable for thin films.[29−37]

In Situ XRD of the Metal-to-Metal Hydride Transition. To address the second aspect of the dissimilar properties exhibited by the $Pd_{1-y}Au_y$ thin films and nanoparticles, the hysteresis, we employed in situ XRD. In Figure 5, the behavior of the ⟨111⟩ diffraction peak as a function of the hydrogen pressure is shown for $Pd_{0.85}Au_{0.15}$, while Figure 6 summarizes the behavior of all-studied $Pd_{1-y}Au_y$ compositions. Clearly, both the film and nanoparticles are textured in the ⟨111⟩ crystallographic direction but their behavior during the phase transition implies distinct structural differences.

In the thin films, increasing the hydrogen pressures leads to a continuous and gradual shift of the ⟨111⟩ diffraction peak to lower diffraction angles [Figure 5a]. This gradual increase of the lattice spacing d_{111} suggests a coherent transition from the dilute $Pd_{1-y}Au_yH_x$ phase to the same phase with a high hydrogen concentration. A similar behavior is observed for all other compositions [Figure 6a−c]. In contrast, the diffractograms of the nanoparticles plotted in Figure 5c show the superposition of two diffraction peaks for hydrogen pressures around P_{H_2} = 1400 Pa. This indicates phase coexistence of α and β-$Pd_{1-y}Au_yH_x$ and thus the occurrence of an incoherent phase transformation for Au concentrations up to at least y = 0.15 for the nanoparticles [Figure S5]. For Au concentrations $y \geq 0.20$, a single phase behavior is observed, as expected from bulk thermodynamics of $Pd_{1-y}Au_y$, where the first-order phase transition disappears above a critical Au fraction of $y \approx 0.18$.[23]

The observed first-order behavior of the phase transition should also be correlated to the hysteresis observed in the lattice constant—and—indeed, we observe a small hysteresis in the lattice constant of the nanoparticles with y = 0.15 [Figure 5d]. Remarkably, the hysteresis extends to y = 0.20 where still a very small hysteresis can be discerned [Figure 6d]. This behavior is in stark contrast to the thin films. While the second-order nature of the transition suggests no hysteresis at all, in fact, we observe it for all compositions [Figure 6a,b]. In addition, this d_{111}-spacing hysteresis extends over a much wider pressure range ($10^1 \lesssim P_{H_2} \lesssim 10^3$), that is, in a similar pressure range as where NR reveals a higher hydrogen solubility [Figure 4]. Apparently, in addition to the first-order phase transformation, there is an additional factor involved inducing hysteresis. It is particularly potent in the thin films and only weakly affects the nanoparticles.

We propose that the different natures of the phase transition in $Pd_{1-y}Au_y$ alloy thin films and nanoparticles are related to substrate clamping. Accommodating hydrogen results in lattice expansion, which induces strains in the host metal lattice. In contrast to bulk materials, two-dimensional clamped films have to obey constraints on lateral expansion, leading to a very high in-plane stress and plastic deformation. As shown by Wagner and Pundt,[36] strong compressive strain may lower the critical temperature of the α-to-β transition, which would explain the single-phase behavior of the PdAu-based thin films. Above the critical temperature, which decreases with increasing Au concentrations [Figure S2],[23,38] there is no distinction between the α and β phases and a solid solution behavior is expected over the whole hydrogenation range. On the other hand, because the nanoparticles are more free to expand laterally, the clamping effects and the related induced lattice strain should be much less pronounced as compared with thin films. Therefore, in the nanoparticles, the first-order α-to-β phase transition occurs under similar conditions as in bulk.

With respect to the observations related to hysteresis, normally its occurrence is related to first-order transitions in which one phase (e.g., the β phase) nucleates in another phase (e.g., the α phase). Hysteresis then occurs due to the energy barriers involved in the nucleation process which prevent the transition to occur at thermodynamic equilibrium.[39−41]

DOI: 10.1021/acsami.8b22455
ACS Appl. Mater. Interfaces 2019, 11, 15489−15497

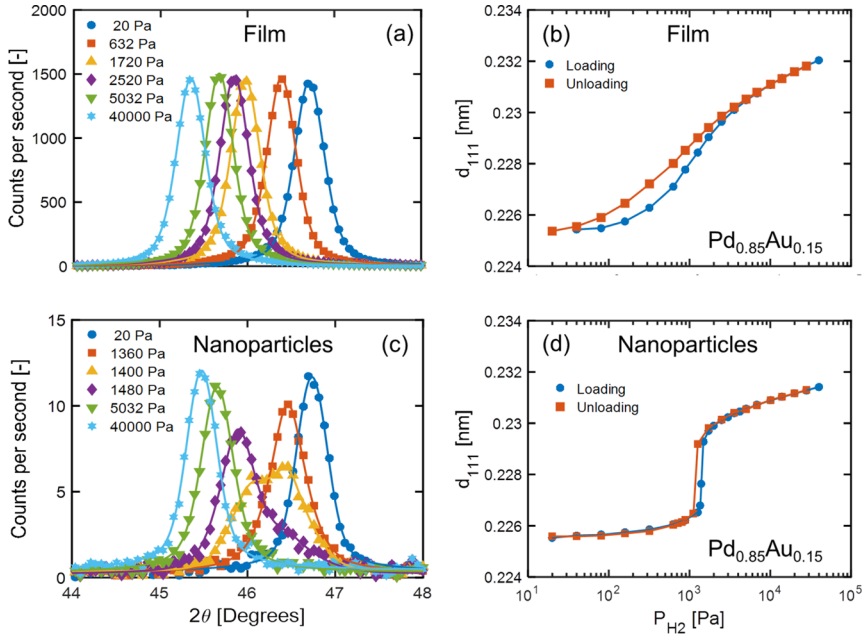

Figure 5. In situ XRD results of (a,b) $Pd_{0.85}Au_{0.15}$ thin films with a 4 nm Ti adhesion layer and (c,d) $Pd_{0.85}Au_{0.15}$ nanoparticles at T = 28 °C. (a,c) Diffractograms of thin film/nanoparticles measured for the hydrogen pressures indicated in the legend and for increasing pressure steps. (b,d) Partial hydrogen pressure dependence of the d_{111}-spacing of a $Pd_{0.85}Au_{0.15}$ thin film/nanoparticles as measured by stepwise increasing and decreasing the pressure. The continuous lines represent fits of a pseudo-Voigt function to the experimental data. As further detailed in this figure, the experimental data of the $Pd_{0.85}Au_{0.15}$ nanoparticles are fitted to a superposition of two pseudo-Voight functions in the region where phase coexistence occurs.

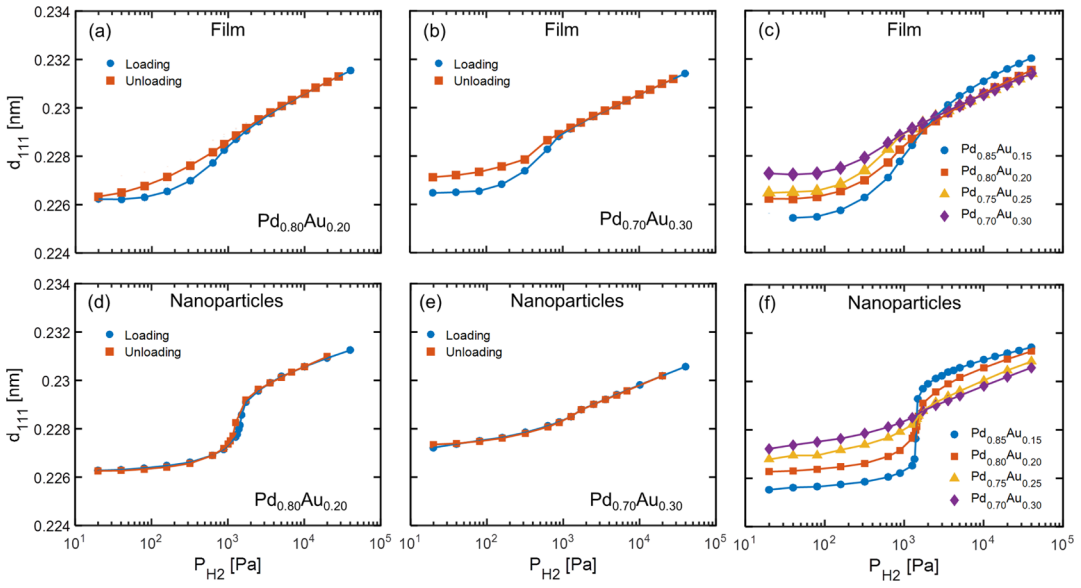

Figure 6. Hydrogen pressure P_{H_2} dependence of the d_{111}-spacing at T = 28 °C as obtained from in situ XRD measurements on (a−c) thin films and (d−f) nanoparticles. (a,d) and (b,e) display the pressure dependence of the d_{111}-spacing of $Pd_{0.80}Au_{0.20}$ and $Pd_{0.70}Au_{0.30}$, respectively, as measured by stepwise increasing and decreasing the partial hydrogen pressure. (c,f) Partial hydrogen pressure dependence of the d_{111}-spacing of $Pd_{1-y}Au_y$ thin films/nanoparticles as measured by stepwise increasing the pressure.

However, here, we find that hysteresis is also present when the first-order behavior and related phase coexistence is completely suppressed. This may be a result of the volumetric expansion required to accommodate the hydrogen absorption. Because this volume change is translated into a thickness increase of the system for which substantial atomic rearrangements have to occur, these rearrangements involve mechanical work and plastic deformation of the film which, in turn, create a thermodynamic barrier that increases the splitting of the hydrogen absorption- and desorption branch of the hydrogenation cycle.[35,36] In addition, the nucleation of domains, inducing locally large stresses, may also be hindered substantially by the clamping of the film to the substrate.[42,43] Our data thus suggest that clamping induces hysteresis in thin films notwithstanding the continuous nature of the phase transition. In the nanoparticles, the clamping is much weaker and hence the hysteresis in the d_{111}-spacing extends to samples just slightly beyond the critical concentration of the first-order

DOI: 10.1021/acsami.8b22455
ACS Appl. Mater. Interfaces 2019, 11, 15489−15497

phase transition. To this end, we also note that clamping may also play an important role in the kinetics of the (de)-hydrogenation process of metal hydrides and may account for the different response times observed between nanoparticles[8,17,19] and thin films,[13] together with the surface-to-volume ratio.

An important observation left unaddressed is the increase of the hydrogen solubility at low pressures in the thin films compared to the nanoparticles [Figure 4]. This effect, at first, is somewhat contradictory to our arguments above because the lattice compression in the thin films should make it more difficult for hydrogen to enter the lattice. In this respect, the expanded d_{111}-spacing [Figure 6] is a result of this uniaxial compression. Hence, we would expect a lower hydrogen concentration in the thin films as compared to the nanoparticles. The opposite is the case, which suggests that the uniaxial compression leads to an enhanced hydrogen absorption. While earlier experiments on comparable systems point in the same direction,[35] further studies are needed to elucidate the details of the origin of this effect. Furthermore, short-ranged atomic order and the number and structure of defects in the material may also play a role.[44] Our results hint that this might be the case, as different hydrogen solubilities are observed for the first and subsequent exposures to hydrogen [Figure S6].

Our results have important implications for the use of PdAu and other metal hydrides in applications such as optical hydrogen sensors. They illustrate that different ways of nanostructuring result in distinctively different sensing characteristics. Consequently, this dissimilar response provides engineers with an additional degree of freedom to tailor the properties of these sensing materials to specific needs. In addition, our results illustrate that one may track the optical transmission of nanoparticles as alternative readout to $\Delta\lambda_{LSPR}$, while maintaining its desirable properties in terms of limited-to-no hysteresis and fast response times [Figure 2d].[17]

In general, the best suited choice of metal hydride, the amount of nanostructuring, and the detection method depend on many factors such as the desired sensing range, operating temperature, response time, and pricing structure. The observation of a higher hydrogen solubility at lower hydrogen pressures ($P_{H_2} \lesssim 10^3$ Pa) of thin films as compared to nanoparticles, and thus a more gradual optical response seems to be a distinct advantage of thin films. Indeed, the gradual and larger response at low pressures possibly results in a higher accuracy and a more pressure independent sensitivity of the hydrogen sensor. However, it comes at the price of increased hysteresis, reducing the accuracy with which one can determine the hydrogen pressure at room temperature. For this reason, $Pd_{1-y}Au_y$ nanoparticles may be a more favorable choice, particularly with y = 0.25 and 0.30. These two compositions have the advantage that they are not prone to the highly undesirable first-order transition for $y \lesssim 0.20$, and that they have a relatively large solubility and optical contrast at especially lower hydrogen pressures [Figure 2].

CONCLUSIONS

In conclusion, we have established the existence of substantial differences between the optical response of $Pd_{1-y}Au_y$ (y = 0.15−0.30) thin films and nanoparticles to hydrogen, even when they have the exact same composition and are measured and analyzed in the same way. Hence, these differences do not result from the method of detection but arise from a different structural response to the hydrogen pressure. Compared with bulk and nanoparticles, thin films exhibit both a larger hydrogen solubility at low hydrogen pressures and a much more pronounced hysteresis, which spans a wider pressure range. These dissimilarities are likely related to the freedom of expansion of the involved system and the clamping of the film to the substrate. Whereas nanoparticles can expand relatively freely in all directions, thin films are confined due to their two dimensional nature and the strong attachment to the support minimizes their ability to reduce stress imposed by hydrogen absorption through lattice strain. Thus, our results empirically suggest that the effect of the substrate clamping on the thin film response to hydrogen exposure is twofold: on the one hand the nature of the phase transition switches from an incoherent first-order transition to a coherent solid solution behavior; however, on the other hand, significant hysteresis between the hydrogen absorption and desorption branch is induced, very likely due to the additional thermodynamic barrier required to undergo the plastic deformations and atomic rearrangements required to accommodate the thickness change. In a wider perspective, our results illustrate that the thermodynamics of nanostructured materials may deviate considerably from continuous thin films and that this is not solely due to surface effects. This provides not only a caveat when utilizing these materials in real-world applications, as, for example, in optical hydrogen sensors or active plasmonic metamaterial devices but also provides an additional degree of freedom to tailor the properties of these materials to specific needs.

METHODS AND MATERIALS

Sample Preparation. *Thin Films.* The $Pd_{1-y}Au_y$ continuous thin films were fabricated by cosputtering without and with a Ti adhesion layer. The 40 nm thick PdAu and 3 nm thick Ti layers were deposited in 3 Pa of Ar by magnetron sputtering in an ultrahigh vacuum chamber (AJA Int.) with a base pressure of 10^{-9} Pa. The samples for the optical and in situ XRD measurements were deposited on 10 × 10 mm^2 quartz substrates with a thickness of 1 mm, while the samples for NR were deposited on 3 mm thick 3″ fused quartz substrates and with a surface roughness < 0.4 nm. The substrates were rotated during the deposition to enhance the homogeneity. Typical deposition rates included 2.5 nm s^{-1} (69 W direct current (dc)) for Pd, 0.5−1.2 nm s^{-1} (10−24 W dc) for Au, and 0.05 nm s^{-1} (100 W dc) for Ti. The thickness of the layers was derived from the sputter rate that was calibrated by stylus profilometry (DEKTAK) on thick samples (>150 nm). The derived thickness is within 10% from the thickness obtained from the neutron and X-ray reflectometry (XRR) measurements (see below). Alternatively, thin film samples were prepared by sputtering layers of Pd and Au on top of each other. These samples were annealed for 2 days in a 96% Ar−4% H_2 atmosphere that was brought from T = 25 to 400 °C and subsequentlyback to 25 °C. Subsequent XRR and XRD measurements confirm a homogenous $Pd_{1-y}Au_y$ layer and optical transmission measurements show a similar response to hydrogen over the entire pressure range as the cosputtered films.

In our analysis, we have considered both thin films with and without 3 nm titanium adhesion layer. In contrast to palladium thin films,[35] the optical response of the second and subsequent exposures to hydrogen is not substantially affected by the inclusion of the Ti adhesion layer [Figure S7], suggesting that the inclusion of gold improves the adhesion to the substrate. In both cases, reproducible results are obtained from the second cycle onward, although the first exposures of the film with and without Ti layers differ considerably [Figure S6]. Differences between the first cycles are common to thin films, as they require, in general, a few cycles of exposure to hydrogen to show reproducible results owing to a settling of the microstructure.

DOI: 10.1021/acsami.8b22455
ACS Appl. Mater. Interfaces 2019, 11, 15489−15497

The similar response for the second and subsequent exposure to hydrogen of the films with and without a Ti adhesion layer is further substantiated by the in situ XRD data, which display a similar evolution of the d_{111}-spacing during the third exposure to hydrogen [Figure S8]. Together with the optical data, these results show that, compared to palladium, the interaction with the substrate strengthens due to the addition of Au, which allows us to make thin film sensors with a high cycling stability (≥140 cycles, see Figure S9). Furthermore, the Ti layer appears to promote the preferential orientation of the PdAu film [Figure S10].

Nanoparticles. Disk-shaped $Pd_{1-y}Au_y$ nanoparticles with a diameter of 190 nm and a thickness of 25 nm were fabricated on glass substrates (Borofloat, Schott Scandinavia AB), following procedures detailed elsewhere.[17,45] A scanning electron microscopy (SEM) micrograph of the nanoparticles is depicted in Figure S11. In short, the fabrication is based on layer-by-layer deposition of Pd and Au films through a quasi-random mask array produced by colloidal lithography. Homogeneous alloying was achieved by annealing at T = 500 °C for 24 h in 4% H_2 in Ar at atmospheric pressures.[45]

Optical Measurements. *Optical Transmission.* The optical transmission was measured using hydrogenography[46] in combination with a three charge-coupled device (3 CCD) camera. The transmission was averaged over an area of 20 × 20 pixels^2, corresponding to 400 mm^2. Five Philips 840 MR16 MASTER LEDs (10/50 W) with a color temperature of 4000 K were used as a (white) light source. The partial hydrogen pressures of $10^{-3} < P_{H_2} < 10^4$ Pa were obtained by using 0.1, 4, and 100% H_2 in Ar gas mixtures. Typical gas flows included 20 sccm for increasing pressure steps and 100 sccm for decreasing pressure steps.

Localized Surface Plasmon Reference. The LSPR hydrogen sensing experiments were carried out in an in-house-made vacuum chamber with UHV-compatible sapphire optical windows.[17,45] The absolute hydrogen pressure was monitored using two capacitive pressure gauges (MKS Baratron Capacitance Manometer). The temperature of the sample was measured using a thermocouple which was in direct contact with the sample surface in combination with a temperature controller (Eurotherm 3216N), which also controlled the heater in the form of a coil wrapped around the chamber. Prior to the measurements, the chamber was flushed multiple times (>10) with a hydrogen-vacuum cycle. The optical transmittance through the sample was measured via a fiber-coupled unpolarized white light source (Avantes AvaLight-Hal) and a fixed grating fiber-coupled spectrometer (Avantes SensLine AvaSpec-2048XL). The LSPR peak position was determined from fitting with an interval of ±60 nm around the maxims in the extinction spectra to a Lorentzian function.

Structural Measurements. *Neutron- and X-ray Reflectometry.* NR measurements were performed at the time-of-flight neutron reflectometers ROG, Reactor Institute Delft, Delft University of Technology, and Offspec, ISIS, Rutherford Appleton Laboratory.[47] The measurements at ROG were performed with an incident angle of 8.5 mrad, a Q-range of 0.10−0.65 nm^{-1}, and a wave-vector resolution of $\Delta Q/Q$ = 0.04. The measurements at Offspec were performed with an incident angle of 8.7 mrad, a Q-range of 0.12−0.90 nm^{-1}, and a wave-vector resolution of $\Delta Q/Q$ = 0.05.

The sample was hydrogenated inside a tailor-made hydrogenation cell with controlled temperature, pressure, and flow. The cell has two aluminum windows to ensure high neutron transmission. Both 0.1 and 4.0% H_2 in Ar gas mixtures were used as a loading gas and a minimum flow of 20 sccm was maintained at all times. The measurements commenced 10 min after changing the pressure to ensure that the sample fully responded to the change in pressure.

Estimates for the layer thickness, roughness, and scattering length density of the $Pd_{1-y}Au_yH_x$ layer were obtained from fitting the NR data using the software package STAR.[48] To obtain estimates of the error bars, boundaries of the confidence intervals of the fitted parameters are computed by finding the value of the parameter of interest for which an F-test shows that the fit with this value differs 1 SD (tail probability of 15.4%) from the value obtained using the best fit. The hydrogen fraction was computed from the fitted parameters by assuming that the number of Pd/Au atoms within the layer remains constant upon hydrogenation (see the Supporting Information of ref 43 for more details). Additional XRR measurements were performed on the as-prepared sample with Rigaku SmartLab (Cu Kα, λ = 0.1542 nm). These measurements were fitted simultaneously with the NR measurements to obtain the most accurate estimates for the initial layer thickness and density of the thin films.

X-ray Diffraction. In situ XRD measurements were performed with a Bruker D8 ADVANCE diffractometer (Co Kα, λ = 0.1789 nm). The sample was hydrogenated at a constant temperature of 28 °C inside an Anton Paar XRK 900 reactor chamber. A gas mixture of 96.0% helium and 4.0% H_2 was used and a constant flow of at least 20 sccm was maintained at all times. After setting and reaching a new pressure set point, we waited 10 min before commencing the XRD measurements in order to be sure that the sample fully responded to the new experimental conditions. The XRD diffractograms are background corrected by subtracting the diffractogram of an empty substrate. The values for the d_{111}-spacing (the out-of-plane direction of the film) and the fwhm were obtained from the best fit of a pseudo-Voigt function to the background-corrected experimental data. The rocking curves were collected around the ⟨111⟩ diffraction peak with a Bruker D8 DISCOVER diffractometer (Cu Kα, λ = 0.1541 nm).

■ ASSOCIATED CONTENT

Supporting Information

The Supporting Information is available free of charge on the ACS Publications website at DOI: 10.1021/acsami.8b22455.

Temperature and hydrogen pressure dependence of the optical response of the thin films; temperature and hydrogen pressure dependence of the optical response of the nanoparticles; typical NR data; typical XRR data; analysis of the XRD data; differences in the optical transmission between the first and subsequent exposure to hydrogen; comparison of the hydrogen pressure dependence of the optical response of thin films with and without a Ti adhesion layer; hydrogen pressure and history dependence of the d_{111}-spacing for thin films with and without a Ti adhesion layer; optical stability of the thin films upon repeated exposure to hydrogen; XRD rocking curves; SEM micrograph of the $Pd_{0.80}Au_{0.20}$ nanoparticles; and d_{111}-spacing of thin films, nanoparticles, and bulk $Pd_{1-y}Au_y$ (PDF)

■ AUTHOR INFORMATION

Corresponding Authors

*E-mail: l.j.bannenberg@tudelft.nl (L.J.B.).
*E-mail: b.dam@tudelft.nl (B.D.).

ORCID

Lars Johannes Bannenberg: 0000-0001-8150-3694
Ferry Anggoro Ardy Nugroho: 0000-0001-5571-0454
Christoph Langhammer: 0000-0003-2180-1379
Bernard Dam: 0000-0002-8584-7336

Notes

The authors declare no competing financial interest.

■ ACKNOWLEDGMENTS

The authors wish to thank the ISIS support staff for their valuable technical assistance. C. de Vroege and B. Boshuizen are acknowledged for renewing the software of the hydrogenation cell for the NR and in situ XRD measurements. The NR experiments at the ISIS Pulsed Neutron and Muon Source were supported by a beamtime allocation from the Science and

DOI: 10.1021/acsami.8b22455
ACS Appl. Mater. Interfaces 2019, 11, 15489−15497

Technology Facilities Council (RB 1700068) and the corresponding data are available at doi.org/10.5286/ISIS.E.86388270. The contributions by F.A.A.N. and C.L. are financially supported by the Swedish Foundation for Strategic Research framework project RMA15-0052 and the Knut and Alice Wallenberg Foundation project 2016.0210.

REFERENCES

(1) Hughes, R. C.; Ricco, A. J.; Butler, M. A.; Martin, S. J. Chemical microsensors. *Science* **1991**, *254*, 74−80.
(2) Butler, M. A. Fiber optic sensor for hydrogen concentrations near the explosive limit. *J. Electrochem. Soc.* **1991**, *138*, L46−L47.
(3) Butler, M. A.; Buss, R. J. Kinetics of the micromirror chemical sensor. *Sens. Actuators, B* **1993**, *11*, 161−166.
(4) Hübert, T.; Boon-Brett, L.; Black, G.; Banach, U. Hydrogen sensors−a review. *Sens. Actuators, B* **2011**, *157*, 329−352.
(5) Perrotton, C.; Javahiraly, N.; Kazemi, A.; Meyrueis, P. Review of optical fiber sensor technologies for hydrogen leak detection in hydrogen energy storage. *Proc. SPIE* **2011**, *8026*, 80260O.
(6) Slaman, M.; Westerwaal, R.; Schreuders, H.; Dam, B. Optical hydrogen sensors based on metal-hydrides. *Proc. SPIE* **2012**, *8368*, 836805.
(7) Javahiraly, N.; Perrotton, C. Hydrogen leak detection: a comparison between fiber optic sensors based on different designs. *Proc. SPIE* **2014**, *9202*, 920206−920211.
(8) Nugroho, F. A. A.; Eklund, R.; Nilsson, S.; Langhammer, C. A fiber-optic nanoplasmonic hydrogen sensor via pattern-transfer of nanofabricated PdAu alloy nanostructures. *Nanoscale* **2018**, *10*, 20533−20539.
(9) Boelsma, C.; Bannenberg, L. J.; van Setten, M. J.; Steinke, N.-J.; Van Well, A. A.; Dam, B. Hafnium - an optical hydrogen sensor spanning six orders in pressure. *Nat. Commun.* **2017**, *8*, 15718.
(10) Wadell, C.; Syrenova, S.; Langhammer, C. Plasmonic hydrogen sensing with nanostructured metal hydrides. *ACS Nano* **2014**, *8*, 11925−11940.
(11) Palm, K. J.; Murray, J. B.; Narayan, T. C.; Munday, J. N. Dynamic optical properties of metal hydrides. *ACS Photonics* **2018**, *5*, 4677−4686.
(12) Zhao, Z.; Carpenter, M. A.; Xia, H.; Welch, D. All-optical hydrogen sensor based on a high alloy content palladium thin film. *Sens. Actuators, B* **2006**, *113*, 532−538.
(13) Westerwaal, R. J.; Rooijmans, J. S. A.; Leclercq, L.; Gheorghe, D. G.; Radeva, T.; Mooij, L.; Mak, T.; Polak, L.; Slaman, M.; Dam, B.; et al. Nanostructured Pd-Au based fiber optic sensors for probing hydrogen concentrations in gas mixtures. *Int. J. Hydrogen Energy* **2013**, *38*, 4201−4212.
(14) Ngene, P.; Westerwaal, R. J.; Sachdeva, S.; Haije, W.; de Smet, L. C. P. M.; Dam, B. Polymer-Induced Surface Modifications of Pd-based Thin Films Leading to Improved Kinetics in Hydrogen Sensing and Energy Storage Applications. *Angew. Chem., Int. Ed.* **2014**, *53*, 12081−12085.
(15) Tang, M. L.; Liu, N.; Dionne, J. A.; Alivisatos, A. P. Observations of shape-dependent hydrogen uptake trajectories from single nanocrystals. *J. Am. Chem. Soc.* **2011**, *133*, 13220−13223.
(16) Jiang, R.; Qin, F.; Ruan, Q.; Wang, J.; Jin, C. Ultrasensitive plasmonic response of bimetallic Au/Pd nanostructures to hydrogen. *Adv. Funct. Mater.* **2014**, *24*, 7328−7337.
(17) Wadell, C.; Nugroho, F. A. A.; Lidström, E.; Iandolo, B.; Wagner, J. B.; Langhammer, C. Hysteresis-free nanoplasmonic Pd−Au alloy hydrogen sensors. *Nano Lett.* **2015**, *15*, 3563−3570.
(18) Yip, H. K.; Zhu, X.; Zhuo, X.; Jiang, R.; Yang, Z.; Wang, J. Gold Nanobipyramid-Enhanced Hydrogen Sensing with Plasmon Red Shifts Reaching 140 nm at 2 vol% Hydrogen Concentration. *Adv. Opt. Mater.* **2017**, *5*, 1700740.
(19) Nugroho, F. A. A.; Darmadi, I.; Zhdanov, V. P.; Langhammer, C. Universal Scaling and Design Rules of Hydrogen-Induced Optical Properties in Pd and Pd-Alloy Nanoparticles. *ACS Nano* **2018**, *12*, 9903−9912.
(20) Nugroho, F. A. A.; Darmadi, I.; Cusinato, L.; Susarrey-Arce, A.; Schreuders, H.; Bannenberg, L. J.; da Silva Fanta, A. B.; Kadkhodazadeh, S.; Wagner, J. B.; Antosiewicz, T. J.; et al. Metal-polymer hybrid nanomaterials for plasmonic ultrafast hydrogen detection. *Nat. Mater.* **2019**, DOI: 10.1038/s41563-019-0325-4.
(21) Lewis, F. A.; Kandasamy, K.; Tong, X. Q. Palladium-hydrogen system. *Solid State Phenom.* **2000**, *73*−*75*, 268−301.
(22) Luo, S.; Wang, D.; Flanagan, T. B. Thermodynamics of Hydrogen in fcc Pd- Au Alloys. *J. Phys. Chem. B* **2010**, *114*, 6117−6125.
(23) Maeland, A.; Flanagan, T. B. X-ray and thermodynamic studies of the absorption of hydrogen by gold-palladium alloys. *J. Phys. Chem.* **1965**, *69*, 3575−3581.
(24) Prinz, J.; Pálsson, G. K.; Korelis, P. T.; Hjörvarsson, B. Combined light and electron scattering for exploring hydrogen in thin metallic films. *Appl. Phys. Lett.* **2010**, *97*, 251910.
(25) Bannenberg, L. J.; Boelsma, C.; Schreuders, H.; Francke, S.; Steinke, N. J.; Van Well, A. A.; Dam, B. Optical hydrogen sensing beyond palladium: hafnium and tantalum as effective sensing materials. *Sens. Actuators, B* **2019**, *283*, 538−548.
(26) Bardhan, R.; Hedges, L. O.; Pint, C. L.; Javey, A.; Whitelam, S.; Urban, J. J. Uncovering the intrinsic size dependence of hydriding phase transformations in nanocrystals. *Nat. Mater.* **2013**, *12*, 905.
(27) Baldi, A.; Narayan, T. C.; Koh, A. L.; Dionne, J. A. In situ detection of hydrogen-induced phase transitions in individual palladium nanocrystals. *Nat. Mater.* **2014**, *13*, 1143.
(28) Griessen, R.; Strohfeldt, N.; Giessen, H. Thermodynamics of the hybrid interaction of hydrogen with palladium nanoparticles. *Nat. Mater.* **2016**, *15*, 311.
(29) Feenstra, R.; Bruin-Hordijk, G. J. d.; Bakker, H. L. M.; Griessen, R.; Groot, D. G. d. Critical point lowering in thin PdHx films. *J. Phys. F: Met. Phys.* **1983**, *13*, L13.
(30) Pundt, A.; Kirchheim, R. Hydrogen in metals: microstructural aspects. *Annu. Rev. Mater. Res.* **2006**, *36*, 555−608.
(31) Janssen, G. C. A. M. Stress and strain in polycrystalline thin films. *Thin Solid Films* **2007**, *515*, 6654−6664.
(32) Wagner, S.; Pundt, A. Mechanical stress impact on thin $Pd_{1-x}Fe_x$ film thermodynamic properties. *Appl. Phys. Lett.* **2008**, *92*, 051914.
(33) Baldi, A.; Gonzalez-Silveira, M.; Palmisano, V.; Dam, B.; Griessen, R. Destabilization of the Mg-H system through elastic constraints. *Phys. Rev. Lett.* **2009**, *102*, 226102.
(34) Pivak, Y.; Gremaud, R.; Gross, K.; Gonzalezsilveira, M.; Walton, A.; Book, D.; Schreuders, H.; Dam, B.; Griessen, R. Effect of the substrate on the thermodynamic properties of PdH_x films studied by hydrogenography. *Scr. Mater.* **2009**, *60*, 348−351.
(35) Pivak, Y.; Schreuders, H.; Slaman, M.; Griessen, R.; Dam, B. Thermodynamics, stress release and hysteresis behavior in highly adhesive Pd−H films. *Int. J. Hydrogen Energy* **2011**, *36*, 4056−4067.
(36) Wagner, S.; Pundt, A. Quasi-thermodynamic model on hydride formation in palladium−hydrogen thin films: Impact of elastic and microstructural constraints. *Int. J. Hydrogen Energy* **2016**, *41*, 2727−2738.
(37) Baldi, A.; Mooij, L.; Palmisano, V.; Schreuders, H.; Dam, B.; Kooi, B. J.; Griessen, R. Elastic versus alloying effects in Mg-based hydride films. *Phys. Rev. Lett.* **2018**, *121*, 255503.
(38) Zhdanov, V. P. A generic statistical model of hydride formation in a random alloy. *Mod. Phys. Lett. B* **2016**, *30*, 1650330.
(39) Wagner, H. Elastic interaction and phase transition in coherent metal-hydrogen alloys. *Top. Appl. Phys.* **1978**, *28*, 5−51.
(40) Flanagan, T. B.; Bowerman, B. S.; Biehl, G. E. Hysteresis in metal/hydrogen systems. *Scr. Metall.* **1980**, *14*, 443−447.
(41) Schwarz, R. B.; Khachaturyan, A. G. Thermodynamics of open two-phase systems with coherent interfaces: Application to metal−hydrogen systems. *Acta Mater.* **2006**, *54*, 313−323.
(42) Mooij, L.; Dam, B. Hysteresis and the role of nucleation and growth in the hydrogenation of Mg nanolayers. *Phys. Chem. Chem. Phys.* **2013**, *15*, 2782−2792.

DOI: 10.1021/acsami.8b22455
ACS Appl. Mater. Interfaces 2019, 11, 15489−15497

(43) Bannenberg, L. J.; Schreuders, H.; van Eijck, L.; Heringa, J. R.; Steinke, N.-J.; Dalgliesh, R.; Dam, B.; Mulder, F. M.; van Well, A. A. Impact of Nanostructuring on the Phase Behavior of Insertion Materials: The Hydrogenation Kinetics of a Magnesium Thin Film. *J. Phys. Chem. C* **2016**, *120*, 10185−10191.
(44) Lee, S.-M.; Noh, H.; Flanagan, T. B.; Luo, S. Hydrogen-induced lattice rearrangement of a $Pd_{0.81}Au_{0.19}$ alloy. *J. Phys.: Condens. Matter* **2007**, *19*, 326222.
(45) Nugroho, F. A. A.; Iandolo, B.; Wagner, J. B.; Langhammer, C. Bottom-up nanofabrication of supported noble metal alloy nanoparticle arrays for plasmonics. *ACS Nano* **2016**, *10*, 2871−2879.
(46) Gremaud, R.; Broedersz, C. P.; Borsa, D. M.; Borgschulte, A.; Mauron, P.; Schreuders, H.; Rector, J. H.; Dam, B.; Griessen, R. Hydrogenography: An Optical Combinatorial Method To Find New Light-Weight Hydrogen-Storage Materials. *Adv. Mater.* **2007**, *19*, 2813−2817.
(47) Dalgliesh, R. M.; Langridge, S.; Plomp, J.; De Haan, V. O.; Van Well, A. A. Offspec, the ISIS spin-echo reflectometer. *Phys. B* **2011**, *406*, 2346−2349.
(48) Van de Kruijs, R. W. E. *Specular and Off-Specular Reflection of Polarized Neutrons from Magnetic Thin Films and Multilayers*; Delft University of Technology, 2002.

DOI: 10.1021/acsami.8b22455
ACS Appl. Mater. Interfaces 2019, 11, 15489−15497